CHEMISTRY
AN ASIAN JOURNAL
ACES
FULL PAPER

DOI: 10.1002/asia.201300496

Adsorption of Polycyclic Aromatic Hydrocarbons on Graphene Oxides and Reduced Graphene Oxides

Yubing Sun,[a] Shubin Yang,[a] Guixia Zhao,[a] Qi Wang,[a] and Xiangke Wang*[b]

Abstract: Graphene has attracted increasing attention in multidisciplinary studies because of its unique physical and chemical properties. Herein, the adsorption of polycyclic aromatic hydrocarbons (PAHs), such as naphthalene (NAP), anthracene (ANT), and pyrene (PYR), on reduced graphene oxides (rGOs) and graphene oxides (GOs) as a function of pH, humic acid (HA), and temperature were elucidated by means of a batch technique. For comparison, nonpolar and nonporous graphite were also employed in this study. The increasing of pH from 2 to 11 did not influence the adsorption of PAHs on rGOs, whereas the suppressed adsorption of NAP on rGOs was observed both in the presence of HA and under high-temperature conditions. Adsorption isotherms of PAHs on rGOs were in accordance with the Polanyi–Dubinin–Ashtahhov (PDA) model, providing evidence that pore filling and flat surface adsorption were involved. The saturated adsorbed capacities (in $mmol\,g^{-1}$) of rGOs for PAHs calculated from the PDA model significantly decreased in the order of NAP > PYR > ANT, which was comparable to the results of theoretical calculations. The pore-filling mechanism dominates the adsorption of NAP on rGOs, but the adsorption mechanisms of ANT and PYR on rGOs are flat surface adsorption.

Keywords: adsorption · graphene · hydrocarbons · reaction mechanisms · surface chemistry

Introduction

The formation of polycyclic aromatic hydrocarbons (PAHs) stems from different ways, such as pyrolysis of petroleum products, incomplete combustion of biomass, and the manufacture of coal tar.[1] Exposures to low-level PAHs in the environment have raised significant attention to concerns about carcinogenic, mutagenic, and teratogenic effects on human health.[2] Thus, it is of great importance to develop efficient treatment technologies for the in situ removal of PAHs in benthic environment cleanup.

Accurate predictions of the fate and transport of PAHs in the environment and in the development of materials suitable for encapsulation and disposal of PAHs require fundamental knowledge of the adsorption behavior of PAHs onto various solid–solution interfaces. Adsorption is superior to other techniques owing to low cost, flexibility and simplicity of design, ease of operation, and insensitivity to organic pollutants. The adsorption of PAHs on various carbonaceous adsorbents (e.g., soot, activated carbon, carbon nanotubes (CNTs), and graphene) has attracted a great deal of research attention in recent years.[3] van Noort et al. found that logarithmic maximum adsorption capacities ($\log Q_{max}$) of activated carbon and graphite were 7.85 and 5.25 $nmol\,g^{-1}$ for phenanthrene, respectively.[3b] Ji et al. found that graphene nanosheets and graphite oxides showed similar sequences of adsorption affinity (in $mmol\,kg^{-1}$): 1-naphthylamine > 2-naphthol > tylosin > naphthalene (NAP).[3k] Graphene nanosheets are regarded as one of the potential superior adsorbents owing to the presence of a huge theoretical surface area ($\approx 2630\,m^2\,g^{-1}$). Zhao et al. also noted that the maximum adsorption capacity (Q_{max}) of sulfated graphene was $2.326\,mmol\,g^{-1}$ for NAP.[4] To the best of our knowledge, there is little information available in the literature about the difference in adsorption of PAHs on graphene oxides (GOs) and reduced graphene oxides (rGOs) under ambient conditions.

The overall objectives of the work described herein were 1) to characterize the microscopic and macroscopic properties of carbonaceous adsorbents by SEM, XRD, Raman spectroscopy, and potentiometric acid–base titration; 2) to elucidate the effects of pH, humic acid (HA), and temperature on NAP adsorption onto GOs and rGOs by means of a batch technique; 3) to discuss the interaction mechanism between PAHs and rGOs; and 4) to simulate the adsorption behaviors of PAHs on rGOs in terms of theoretical calculations. This study highlighted the adsorption mechanism between PAHs and rGOs with a combination of macroscopic adsorption and theoretical calculation methods.

[a] Y. Sun, S. Yang, G. Zhao, Q. Wang
Key Laboratory of Novel Thin Film Solar Cells
Institute of Plasma Physics
Chinese Academy of Science
P.O. Box 1126, Hefei, 230031 (P.R. China)

[b] X. Wang
School for Radiological and Interdisciplinary Sciences
Soochow University
Suzhou, 215123, P.R. China
E-mail: xkwang@ipp.ac.cn

Supporting information for this article is available on the WWW under http://dx.doi.org/10.1002/asia.201300496.

Results and Discussion

Characterization of Carbonaceous Adsorbents

The results obtained for characterization by SEM, XRD, and Raman spectroscopy are given in Figure 1. The SEM images (Figure 1 A and B) show that GOs and rGOs are

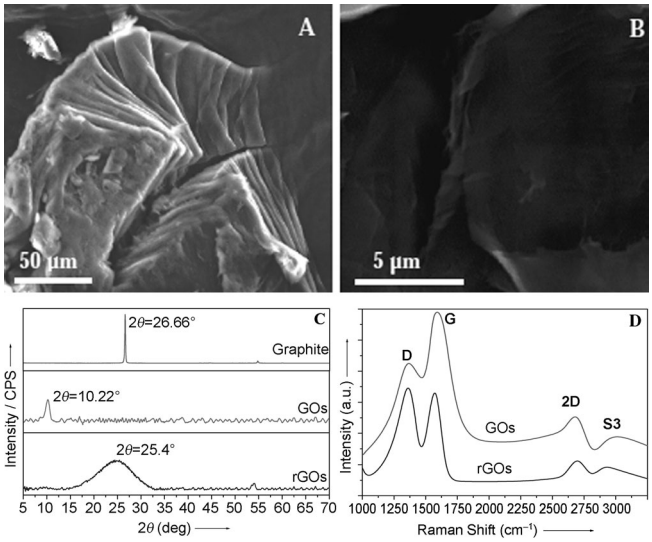

Figure 1. Characterization of the carbonaceous adsorbents: SEM images of rGOs (A) and GOs (B); C) XRD patterns of graphite, GOs, and rGOs; and D) Raman spectra of rGOs and GOs.

randomly aggregated and agglomerated together. The XRD patterns of graphite and GOs (Figure 1 C) indicate that the *c* axis spacing increases from 0.334 (corresponding to the diffraction peak at $2\theta = 26.66°$) to 0.865 nm (corresponding to the diffraction peak at $2\theta = 10.22°$) during the oxidation process owing to the formation of oxygen-containing functional groups (−OH, −COOH, −O−, −CHO, etc.) on the surface of the GOs.[5] For rGOs, the reappearance of the weak and broad diffraction peak at $2\theta = 25.40°$ is attributed to the rather limited ordering in each rGO nanosheet and the uneven interlayer spacing over the whole rGO sample.[6] According to Raman spectroscopy, the G band ($\approx 1580\ cm^{-1}$) and D band ($\approx 1350\ cm^{-1}$) of GOs and rGOs are observed (Figure 1 D); these are related to the vibration of sp^2-carbon atoms in a graphitic 2*D* hexagonal lattice and the vibrations of sp^3-carbon atoms of defects and disorder, respectively.[7] The weak and broad 2D band (from two phonons with opposite momentum in the highest optical branch) at about $2700\ cm^{-1}$ is also an indication of disorder as a result of an out-of-plane vibration model, which is similar to the results of previous reports.[8] The significant decrease in the relative intensity of the low-frequency 2D bands shows a further increase in the layers of GOs and rGOs.[9] The G band position of GOs is about $100\ cm^{-1}$ higher than that of rGOs. This upshift is partially due to chemical doping (occurrence of substantial oxygen functional groups on the surface of GOs).[10] According to the results of potentiometric acid–base titration, the pH_{PZC} (pH at point of zero charge) values of GOs and rGOs are 3.9 and 7.1, respectively (Table S1 in the Supporting Information).

pH Effect

The adsorption of NAP on rGOs, GOs, and graphite over the relatively wide range of pH from 2.0 to 11.0 is shown in Figure 2 A. The adsorption of NAP on graphite and rGOs is

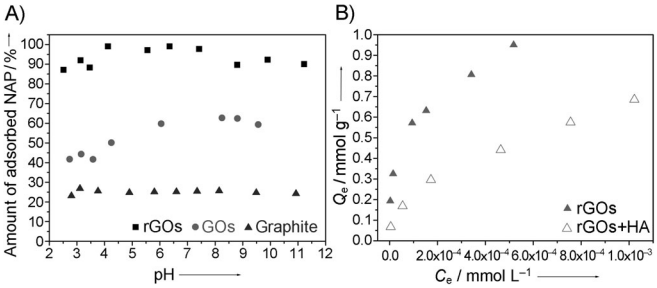

Figure 2. A) The effect of pH on NAP adsorption onto graphite, GOs, and rGOs; $C_{NAP} = 0.1\ mmol\,L^{-1}$, $I = 0.01\ mol\,L^{-1}$ $CaCl_2$, $T = (25 \pm 1)$ °C. B) The effect of HA on pyrene (PYR) adsorption onto rGOs; pH 6.5 ± 0.1, $I = 0.01\ mol\,L^{-1}$ $CaCl_2$, $C_{HA} = 10\ mg\,L^{-1}$, $T = (25 \pm 1)$ °C.

independent of pH, whereas pH-dependent adsorption of NAP on GOs is observed at low pH values. The pH-independent adsorption of NAP onto graphite and rGOs is consistent with the adsorption of NAP on phospholipids[11] and on single-walled CNTs.[12] About 95, 60, and 25 % of NAP is adsorbed onto the rGO, GO, and graphite surface, respectively, under neutral pH conditions; this suggests that rGOs have a larger adsorption capacity for PAHs than that of GOs and graphite.

The differences in adsorption capacities between rGOs and GOs result from the structures and surface properties of the adsorbents, for example, the formation of micropores and deprotonation of surface functional groups.[3j] The formation of micropores in the rGOs is attributed to its porosity, lattice vacancies, and dislocations, which may create heterogeneous sites with different adsorption energies for the adsorption of PAHs.[13] For GOs, the increase in pH over a relatively wide range facilitates deprotonation of acidic functional groups (−COOH, −OH) of GOs, which promotes the π-electron-donor ability of the graphene surface under low pH conditions. The carboxyl group (−COOH) is a weak electron donor and acceptor, whereas −COO− is a strong electron donor, but not an acceptor.[12] For the weak π donors of NAP, pH-dependent adsorption of NAP on GOs at low pH values is attributed to π-electron donor–acceptor interactions. At high pH, however, a subtle change in the adsorption of NAP on GOs is observed, and it is assumed that hydrophobic interactions dominate the adsorption behavior under high pH conditions. Therefore, the effect of pH on NAP adsorption cannot simply be attributed to the changes in the hydrophilicity of functional groups.[11] For graphite, which is only composed primarily of series of

stacked parallel layer planes, trigonal sp^2 bonding is observed; therefore, the graphite has a lower adsorption capacity for hydrophobic organic compounds compared with rGOs and GOs.

HA Effect

The presence of natural organic matter (NOM), such as HA, influences the removal of PAHs from aqueous solutions.[14] It is hypothesized that two types of carbon NOM ("soft" and "hard" carbon) are observed. Sorption of PAHs into the soft-carbon NOM follows a nearly linear partitioning process, whereas sorption on hard-carbon NOM exhibits both adsorption and absorption or partitioning. As shown in Figure 2B, the presence of HA reduces the adsorption of PAHs on rGOs, which could be caused by competitive adsorption between PAHs and HA onto rGOs. There are two possible reasons for this: 1) high affinity for PAH molecules; 2) fouling of HA on the surface of rGOs. It has been documented previously that HA molecules contain long, flexible aliphatic chains, which would show high affinity to rGOs, probably owing to strong electrostatic interactions. In contrast to the aliphatic chain, aromatic rings in PAH molecules are hard and inflexible. It is believed that the binding of PAHs to HA is dominated by van der Waals type interactions.[15] Schlautman and Morgan found that the binding of PAHs to HA was significantly influenced by the steric characteristics of the molecule, which controlled its ability to fit into the hydrophobic cavities of the organic structure.[14c] The results are consistent with the results of PYR adsorption on granulated activated carbon; Radian and Mishael found that the adsorption of PYR by granulated activated carbon decreased dramatically from 80% to less than 2% with increasing HA concentration from 1 to 10 mg L^{-1}.[14h]

Adsorption Isotherms

The adsorption isotherms of PYR on rGOs, GOs, and graphite are shown in Figure 3. The adsorption capacity of PYR on rGOs, GOs, and graphite significantly decreases in the order of rGOs > GOs ⋙ graphite. The oxygen-containing functional groups (−OH, −COOH, −O−, −CHO, etc.) of GOs can form hydrogen bonds with water molecules, which can consequently make GOs more hydrophilic to suppress the adsorption of PAHs through competition with water molecules.[16] Consequently, the adsorption capacity of PAHs on GOs is lower than that of PAHs on rGOs, which is in line with the previously mentioned report for oxidized and pristine CNTs (K_F values were 21.4 and 36.1 $(mg\,g^{-1})/(mg\,L^{-1})^n$ for oxidized and pristine multiwalled carbon nanotubes (MWCNTs), respectively).[17] Pan and Xing also demonstrated that the adsorption of PAHs on CNTs decreased with increasing oxygen content of graphene nanosheets owing to the depressed hydrophobic interaction.[18]

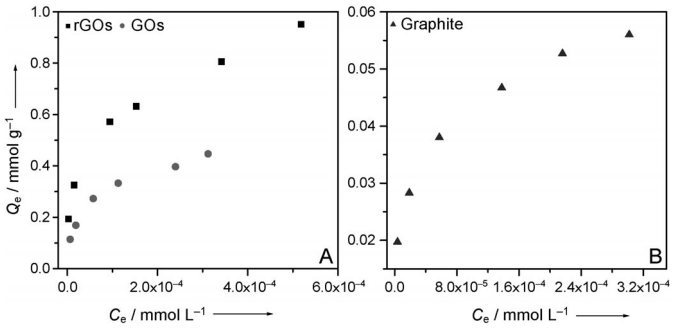

Figure 3. A) Adsorption isotherms of PYR on rGOs and GOs; pH 6.5 ± 0.1, I = 0.01 mol L^{-1} $CaCl_2$, T = (25 ± 1) °C. B) Adsorption isotherms of PYR on graphite; pH 6.5 ± 0.1, I = 0.01 mol L^{-1} $CaCl_2$, T = (25 ± 1) °C.

The Effect of Aromatic Rings

Experiments for the adsorption of three PAHs (NAP, ANT, and PYR) on rGOs were also conducted in this study to examine the effect of different aromatic rings on the adsorption of PAHs from aqueous solutions (Figure 4A). The rate

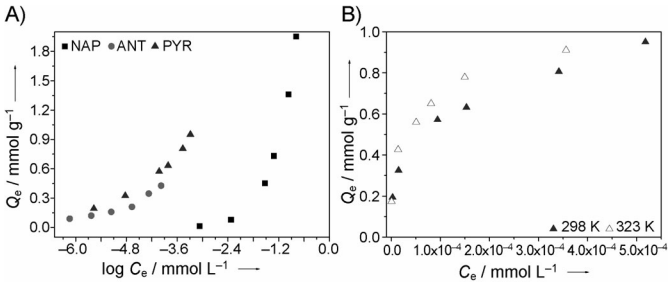

Figure 4. Adsorption isotherms of NAP, ANT, and PYR on rGOs (A) and the effect of temperature on the adsorption of PYR onto rGOs (B); I = 0.01 mol L^{-1} $CaCl_2$, T = (25 ± 1) °C.

and extent of NAP adsorption on rGOs is enhanced relative to those of ANT and PYR (Figure 4A); this is attributed to the surface properties of rGOs and the properties of PAHs. The given rGOs could not be occupied by large organic molecules because of strong heterogeneity.[16] The larger molecule of PYR has a lower adsorption capacity in the pores of rGO aggregates than the relatively smaller molecules (e.g., NAP and ANT) because of the bottleneck of pores (aggregation of graphene nanosheets) for organic chemical diffusion.[19] More specifically, PAHs with more aromatic rings in their molecules have higher π* values and lower water solubilities (Table S2 in the Supporting Information),[20] thereby the lowest adsorption of ANT on rGOs is observed in this study.

Isotherm fitting with Langmuir, Freundlich, and Polanyi–Dubinin–Ashtakhov (PDA) models was conducted, and consequently, parameters calculated from the isotherms are summarized in Table 1. Isotherms for all PAHs correspond very well to the PDA model; this provides evidence that pore filling and flat surface adsorption is involved. The fitting results were consistent with the results reported by Wang et al.,[21] who found that the adsorption data of NAP

Table 1. Results of fitting Langmuir, Freundlich, and PDA models to the adsorption data of PAHs on carbonaceous adsorbents.

Samples	Langmuir			Freundlich			PDA		
	Q_{max} [mmol g^{-1}]	K_L [L mmol^{-1}]	R^2	K_F [(mmol g^{-1})/(mmol g^{-1})^n]	$1/n$	R^2	Q^0 [mmol g^{-1}]	E [kJ mol^{-1}]	R^2
graphite+PYR	0.058	42860	0.992	0.1222	0.242	0.999	0.530	15.73	0.999
GOs+PYR	0.476	30018	0.989	100.925	0.346	0.992	1.050	25.09	0.999
rGOs+PYR	0.979	69.47	0.976	153.816	0.298	0.998	4.842	19.04	0.998
rGOs+ANT	0.454	73353	0.963	87.096	0.312	0.978	1.028	16.14	0.999
rGOs+NAP	5.981	2.858	0.966	262.422	0.928	0.998	46.132	10.25	0.999

on CNTs fitted to the PDA model very well. As illustrated in Table 1, the saturated adsorbed capacities (in mmol g^{-1}) of rGOs for PAHs calculated from the PDA model significantly decreased in the order of NAP > PYR > ANT, which is consistent with the maximum adsorption capacity calculated from the Langmuir model. It is observed that the degree of heterogeneity ($1/n$, calculated from the Freundlich model) of PYR on rGOs is higher than that of graphite, suggesting that more homogeneous adsorption sites are observed on the surface of rGOs. The aggregated structure of rGOs results from its strong hydrophobicity, which may create heterogeneous sites with different adsorption energies for PAHs. The heterogeneous sites of rGOs may stem from the following types: 1) in the interstitial spacing between neighboring graphene nanosheets; and 2) on the curved surface of the periphery of nanosheets.[3j] From a literature survey (Table 2), the logarithmic Freundlich adsorption coefficients of NAP, ANT, and PYR on rGOs (K_F = 15.92, 247.17, and 369.06 (mg g^{-1})/(mg L^{-1})^n for NAP, ANT, and PYR, respectively) are comparable to other adsorbents used to adsorb PAHs from aqueous solutions, such as activated carbon (K_F = 45.71, 331.13, and 187.75 (mg g^{-1})/(mg L^{-1})^n for NAP,[17] ANT,[22b] and PYR,[22c] respectively), MWCNTs (K_F = 12.88 and 234.42 (mg g^{-1})/(mg L^{-1})^n for NAP[22d] and PYR[21] respectively), activated sludge[22b] (K_F = 0.24 and 20.42 (mg g^{-1})/(mg L^{-1})^n for NAP[22a] and PYR,[22a] respectively) and quartz (K_F = 0.36 (mg g^{-1})/(mg L^{-1})^n for PYR[22e]). From the results of the interaction of PAHs with rGOs, one can see that rGOs can be used as a suitable material for the removal of hydrophobic organic compounds in environmental pollution clean up. Although rGOs are relatively expensive compared with activated carbon, rGOs will be synthesized at a lower price and on a larger scale in the near future with the development of new technology. The high adsorption capacity of rGOs for PAHs makes their application in hydrophobic organic compound management promising.

Table 2. Comparison of logarithmic Freundlich adsorption coefficients of the adsorption of PAHs on various adsorbents.

Adsorbents	Adsorbate	K_F [(mg g^{-1})/(mg L^{-1})^n]	Ref.
activated carbon	NAP	212.8	[17]
oxidized MWCNTs	NAP	9.4	[17]
activated sludge	NAP	0.24	[22b]
rGOs	NAP	15.92	this study
activated carbon	ANT	331.13	[22c]
rGOs	ANT	247.17	this study
activated carbon	PYR	187.75	[22d]
MWCNTs	PYR	234.42	[22a]
quartz	PYR	0.36	[22e]
activated sludge	PYR	20.42	[22b]
rGOs	PYR	369.06	This study

Temperature Effect

The effect of temperature on the adsorption of PYR onto rGOs from the aqueous phase is given in Figure 4B. The adsorption of PYR on rGOs decreases with increasing temperature, which is in accordance with the adsorption of PYR on both laboratory- and field-contaminated sediment.[23] Sleep and McClure also found that the adsorption of NAP on soil decreased by 60% as the temperature increased from 22 to 90 °C.[24] He et al. also found that the adsorption of fluoranthene on soil and lava decreased as the temperature increased from 15 to 35 °C.[25] The temperature could potentially affect the adsorption behavior in two ways: 1) diffusivities in solution and interstitial water change with temperature, but a change in temperature only influences about a 10% range in molecular diffusivities; and 2) temperature can change the partition coefficients, and consequently, change the diffusivities. The adsorption processes combine a negative temperature dependence of the equilibrium of fast adsorption and a positive temperature dependence on the kinetics of slow adsorption.[26] The aforementioned results indicate that the equilibrium of fast adsorption dominates the adsorption of PYR on rGOs.

Interaction Mechanism

For hydrophobic organic compounds without any polar groups, such as PAHs, the main driving force behind the adsorption process is hydrophobic adsorption.[27] As described previously for adsorption isotherms, the adsorption of PAHs on carbonaceous adsorbents can be fitted by the Freundlich model very well, although this model cannot separately describe the partition and adsorption mechanisms.[19,28] In recent years, Polanyi-based models were employed to simulate the adsorption of hydrophobic organic compounds on carbonaceous adsorbents extensively,[3d,e,15b,18,29] by assuming that the adsorption behavior of hydrophobic organic compounds could be described by pore filling and flat surface adsorption. The adsorption mechanism of NAP by rGOs can be dominated by pore filling because there are large numbers of high-energy sites in micropores, such as nano-

sheet defects, functional groups, and interstitial and grooves region between graphene nanosheets. The stronger suppression of the adsorption of PYR by rGOs in comparison with NAP was due to its larger molecular size; thus, it would be able to block more micropores and reduce the availability of adsorption sites for PYR adsorption. The suppressed adsorption of ANT on rGOs could be attributed to limited solubility in aqueous solution. Therefore, the adsorption of ANT and PYR on rGOs would be dominated by the surface-adsorption mechanism because there are limited sites in the pores for large molecules.

The adsorption of NAP, ANT, and PYR on rGOs can be theoretically modeled by using the Metropolis Monte Carlo method.[30] The Metropolis Monte Carlo method assumes that the adsorbate molecules do not have a high degree of torsional flexibility and ignores any internal degrees of freedom that the adsorbate components may possess on the substrate surface. The results of theoretically modeling are shown in Figure 5. NAP, ANT, and PYR molecules are adsorbed on the rGOs surface in a tilted form with one stable state. Based on the modeled results, the most stable stacked structures of NAP, ANT, and PYR on the surface of the rGOs are 3.389, 3.447, and 3.455 Å, respectively, above the surface of the rGOs with a total energy of 18.583, 27.316, and 29.676 kcal mol^{-1}, respectively. The binding energy between PAHs and rGOs increases with an increasing number of aromatic rings, which is agreement with the previous study.[31] The enhancement of the binding energy is disproportionate to the actual number of aromatic rings. Chakarova-Käck et al. also found that the binding energy of PAH dimers (i.e., NAP, ANT, and PYR) versus the number of cyclic rings showed nonlinear scaling. [32] A number of quantum chemistry calculations are available for PAH polymers, such as di- or trimers, but no current calculated results can offer a direct comparison to our calculations.[33] The PAH dimer results can be extrapolated to the properties of a graphene dimer. The increase in the binding energy means a decrease in the adsorption capacities between PAHs and rGOs; this indicates that the adsorption of PAHs on rGOs gradually decreased with an increasing number of aromatic rings. The results from theoretical calculations are consistent with our experimental results.

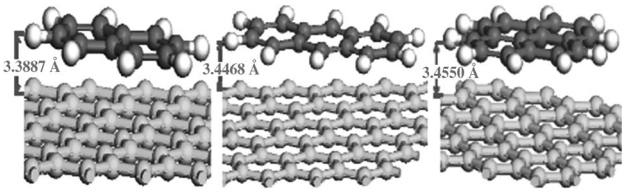

Figure 5. Side views of NAP, ANT, and PYR on the surface of rGOs.

Conclusion

The adsorption of PAHs (i.e., NAP, ANT, and PYR) on rGOs as a function of pH, HA, initial concentration, and temperature was investigated by batch techniques. The suppressed adsorption of NAP on rGOs was observed both in the presence of HA and under high-temperature conditions, whereas increasing the pH from 2 to 11 did not influence the adsorption of PAHs on rGOs. The adsorption isotherms of PAHs on rGOs fitted well with the PDA model, and the saturated adsorbed capacities (mmol g^{-1}) of rGOs for PAHs calculated from the PDA model significantly decreased in the order of NAP > PYR > ANT; this was comparable to the results of theoretical calculations. The pore-filling mechanism dominates the adsorption of NAP on rGOs, but the flat surface adsorption is the main adsorption mechanism for ANT and PYR.

Experimental Section

Materials

The GOs were synthesized by a modified Hummer method,[34] and rGOs were obtained by reduction of GOs under hydrazine hydrate conditions.[35] Briefly, flaked graphite was strongly oxidized by using $KMnO_4$ and concentrated H_2SO_4 under vigorous stirring conditions, and excess oxidative agents were eliminated by using H_2O_2 (30% aqueous solution). The GOs were obtained by centrifugation at 18000 rpm for 30 min and repeated rinsing with Milli-Q water. The rGOs were obtained by using hydrazine hydrate as a reducing agent. Detailed processes for the syntheses of GOs and rGOs are given in the Supporting Information. The preparation and characterization of GOs and rGOs was also described in detail in our previous papers.[4,36,37]

The physicochemical properties of PAHs are reported in Table S1 in the Supporting Information. Stock solutions of NAP, ANT, and PYR at 0.5 g L^{-1} were prepared from solutions of NAP, ANT, and PYR (purity 99.99%) in methanol, followed by dilution with a 0.1 mol L^{-1} solution of $CaCl_2$ to keep the methanol content in the test solution below 0.1% to minimize the effect of cosolvent on the interaction of PAHs with GOs or rGOs. HA extracted from peat soil (Huajia, P.R. China) was characterized previously,[38] and a stock solution was prepared by dissolving it in a 0.1 mol L^{-1} solution of NaOH. Analytical grade chemicals were supplied by Sigma–Aldrich Chemicals, and used directly without further purification in this study.

Characterization of GOs and rGOs

The GOs and rGOs were characterized by SEM, XRD, Raman spectroscopy, and potentiometric acid–base titration. The SEM images were obtained on a field-emission scanning electron microscope (FEI-JSM 6320F). Graphite, GOs, and rGOs were mounted for XRD analysis with a Rapid-II powder diffractometer (D/RAPID II, Japan) using $Cu_{K\alpha}$ radiation ($\lambda = 0.15406$ nm) with a 0.02° step size and a 2 s step time. The potentiometric acid–base titrations were performed by using a computer-controlled titration system (DL50 Automatic Titrator, Mettler Toledo). Briefly, these carbonaceous adsorbents were spiked into 0.01 mol L^{-1} $NaClO_4$ background electrolyte at room temperature, and purged with argon gas to exclude atmospheric CO_2 (g). The initial pH of the suspension was adjusted to acidic conditions (pH ≈ 3.0) by adding a solution of $HClO_4$ under vigorous stirring, and then the suspension was slowly titrated to alkaline conditions (pH ≈ 11.0) with normalized NaOH titrant at variable increments. The data sets of pH versus the net consumption of H^+ or OH^- were used to obtain intrinsic acidity constants (Figure S1 in the Supporting Information).

Adsorption Experiments

The adsorption of NAP, ANT, and PYR on adsorbents (GOs, rGOs, and graphite) was carried out in glass centrifuge tubes with aluminum foil lined Teflon screw caps to prevent degradation of PAHs during adsorption experiments. Vials received various amount of rGOs, GOs, and graphite with a sufficient volume (10 mL) of 0.01 mg L^{-1} background electrolyte ($NaClO_4$ solution) containing 200 mg L^{-1} NaN_3 (as the bioinhibitor). The initial concentration ranges were 2.0×10^{-4} to 0.24 mmol L^{-1} for NAP, 1.0×10^{-5} to 2.5×10^{-4} mmol L^{-1} for ANT, and 1.0×10^{-5} to 6.4×10^{-4} mmol L^{-1} for PYR. The solid–liquid ratios of rGOs/GOs and graphite were 0.2 and 0.4 g L^{-1}, respectively. The pH of the suspensions was adjusted to be in the range 2.0 to 11.0 by adding negligible volumes of 0.05 mol L^{-1} HNO_3 or 0.1 mol L^{-1} NaOH solution by using a glass combination electrode (pH/conductivity meter, Fisher Scientific), but the pH values after equilibrium were used in this study. All of the vials (no head space) with aluminum foil lined Teflon screw caps were continuously shaken on an air-bath shaker at room temperature for 7 days. Our preliminary test showed that adsorption equilibrium was reached within 5 days (data not shown). At the end of adsorption equilibrium, the suspensions were centrifuged at 3000 rpm for 30 min. The blank experiments (without GOs, rGOs, and graphite) were included in each set of adsorption experiments to eliminate mass losses during experimental processes by assuming that these were proportional to the final aqueous concentrations.[39] The concentrations of NAP, ANT, and PYR were analyzed directly by HPLC (HPLC 1200, Agilent Technologies, US). Isocratic elution with a UV detector was performed under the following conditions: 75% methanol/25% water (v/v) with a wavelength of $\lambda=254$ nm for NAP. Isocratic elution with a fluorescence detector was conducted under the following conditions: 90% methanol/10% water with excitation/emission wavelengths of $\lambda=355/402$ and 334/391 nm for ANT and PYR, respectively;[11] Solid-phase concentrations were estimated by the difference between initial concentration references and the corresponding equilibrium aqueous-phase concentrations. All experimental data were the average of triplicate determinations and the relative errors were about $\pm5\%$.

Isotherm Models

The Langmuir [Eq. (1)], Freundlich [Eq. (2)], and PDA [Eq. (3)] models[40] were used for data fitting in this study.

$$\text{Langmuir model}: \quad Q_e = Q_{max}K_L C_e/(1+K_L C_e) \tag{1}$$

$$\text{Freundlich model}: \quad \log Q_e = \log K_F + 1/n \log C_e \tag{2}$$

$$\text{PDA model}: \quad \log Q_e = \log Q^0 - (\varepsilon_{sw}/E)^b \tag{3}$$

in which Q_e and C_e are equilibrium solid- (in mmol g^{-1}) and liquid-phase (in mmol g^{-1}) concentrations, respectively; K_L (in L mmol^{-1}) and K_F (in (mg g^{-1})/(mg L^{-1})^n) are the Langmuir and Freundlich adsorption coefficients, respectively; Q_{max} (in mmol g^{-1}) and Q^0 (in mmol g^{-1}) are the maximum adsorption capacity and the saturated adsorbed capacity of solute, respectively; $1/n$ is often used as an indicator of isotherm nonlinearity; ε_{sw} $(=RT\ln(C_s/C_e))$, in kJ mol^{-1}) and E (in kJ mol^{-1}) are effective adsorption potential and correlating divisor, respectively; R is the universal gas constant; T (in K) is the absolute temperature; and b is the fitting parameter.

Theoretical Calculations

For the adsorption of NAP, ANT, and PYR on the graphene system, the configuration could be constructed by using the adsorption computer code of Material Studio; the Metropolis Monte Carlo method was used to search for adsorption configurations. In this method, the positions and orientations of the PAH molecules were sampled. The periodic boundary conditions (6×6 matrix, related surface area of 14.76×14.76 Å^2, the height of 25 Å) were chosen to ensure that the distance between two adjacent graphene sheets was large enough to avoid interactions between them. For simulations of the graphene/PAH system, the COMPASS force field was designed to detect structural deviations from known properties of the interlayer region. The COMPASS force field provided the potential energy equation and all valence and van der Waals interaction parameters employed in subsequent simulations.[41] The cutoff distance for van der Waals interactions was 17.7 Å. Long-range electrostatic interactions and short-range van der Waals interactions were summed by using the group and atom-based summation methods, respectively.

Acknowledgements

Financial support from the National Natural Science Foundation of China (21207135, 21071107, and 21225730) and 973 projects from the Ministry of Science and Technology of China (2011CB933700) are acknowledged.

[1] a) C. Achten, T. Hofmann, *Sci. Total Environ.* **2009**, *407*, 2461–2473; b) S. Hale, J. Lehmann, D. Rutherford, A. Zimmerman, R. Bachmann, V. Shitumbanuma, A. O'Toole, K. Sundqvist, H. Arp, G. Comelissen, *Environ. Sci. Technol.* **2012**, *46*, 2830–2838.
[2] a) D. Arfsten, D. Schaeffer, D. Mulveny, *Ecotoxicol. Environ. Saf.* **1996**, *33*, 1–24; b) J. Djomo, A. Dauta, V. Ferrier, J. Narbonne, A. Monkiedje, T. Njine, P. Garrigues, *Water Res.* **2004**, *38*, 1817–1821.
[3] a) T. Bucheli, O. Gustafsson, *Environ. Sci. Technol.* **2000**, *34*, 5144–5151; b) P. van Noort, M. Jonker, A. Koelmans, *Environ. Sci. Technol.* **2004**, *38*, 3305–3309; c) R. Lohmann, J. MacFarlane, P. Gschwend, *Environ. Sci. Technol.* **2005**, *39*, 141–148; d) K. Yang, L. Zhu, B. Xing, *Environ. Sci. Technol.* **2006**, *40*, 1855–1861; e) X. Wang, T. Sato, B. Xing, *Environ. Sci. Technol.* **2006**, *40*, 3267–3272; f) P. Liu, D. Zhu, H. Zhang, X. Shi, H. Sun, F. Dang, *Environ. Pollut.* **2008**, *156*, 1053–1060; g) X. Qu, P. Liu, D. Zhu, *Environ. Sci. Technol.* **2008**, *42*, 1109–1116; h) D. Zhu, H. Zhang, Q. Tao, Z. Xu, S. Zheng, *Environ. Toxicol. Chem.* **2009**, *28*, 1400–1408; i) K. Yang, B. Xing, *Chem. Rev.* **2010**, *110*, 5989–6008; j) W. Wu, W. Chen, D. Lin, K. Yang, *Environ. Sci. Technol.* **2012**, *46*, 5446–5454; k) L. Ji, W. Chen, Z. Xu, S. Zheng, D. Zhu, *J. Environ. Qual.* **2013**, *42*, 191–198.
[4] G. Zhao, X. Jiang, Y. He, J. Li, H. Dong, X. Wang, *Adv. Mater.* **2011**, *23*, 3959–3963.
[5] D. Long, W. Li, L. Ling, J. Miyawaki, S. Yoon, *Langmuir* **2010**, *26*, 16096–16102.
[6] X. Fan, W. Peng, Y. Li, X. Li, S. Wang, G. Zhang, F. Zhang, *Adv. Mater.* **2008**, *20*, 4490–4493.
[7] G. Eda, M. Chhowalla, *Adv. Mater.* **2010**, *22*, 2392–2415.
[8] V. Tung, M. Allen, K. Yang, R. Kaner, *Nat. Nanotechnol.* **2009**, *4*, 25–29.
[9] L. Cançado, M. Pimenta, B. Neves, G. Medeiros-Ribeiro, T. Enoki, Y. Kobayashi, K. Takai, K. Fukui, M. Dresselhaus, *Phys. Rev. Lett.* **2004**, *93*, 047403.
[10] A. Ferrari, J. Meyer, V. Scardaci, C. Casiraghi, M. Lazzeri, F. Mauri, S. Piscanec, D. Jiang, K. Novoselov, S. Roth, A. Geim, *Phys. Rev. Lett.* **2006**, *97*, 187401.
[11] X. Qu, X. Wang, D. Zhu, *Environ. Sci. Technol.* **2007**, *41*, 8321–8327.
[12] J. Chen, W. Chen, D. Zhu, *Environ. Sci. Technol.* **2008**, *42*, 7225–7230.
[13] H. Pierson, *Handbook of Carbon, Graphite, Diamond and Fullerenes: Properties, Processing and Applications*, Noyes Publications, Park Ridge, NJ, **1995**, pp. 43–68.
[14] a) C. Chiou, L. Peters, V. Freed, *Science* **1979**, *206*, 831–832; b) S. Karickhoff, D. Brown, T. Scott, *Water Res.* **1979**, *13*, 241–248; c) M. Schlautman, J. Morgan, *Environ. Sci. Technol.* **1993**, *27*, 961–969; d) B. Raber, I. Kogelknabner, *Eur. J. Soil Sci.* **1997**, *48*, 443–455; e) B. Chefetz, A. Deshmukh, P. Hatcher, E. Guthrie, *Environ. Sci. Technol.* **2000**, *34*, 2925–2930; f) Y. Laor, M. Rebhun, *Environ. Sci. Technol.* **2002**, *36*, 955–961; g) B. Wen, J. Zhang, S. Zhang, X. Shan, S. Khan, B. Xing, *Environ. Sci. Technol.* **2007**, *41*, 3165–3171; h) A. Radian, Y. Mishael, *Environ. Sci. Technol.* **2012**, *46*, 6228–6235.

[15] a) T. Gauthier, W. Seitz, C. Grant, *Environ. Sci. Technol.* **1987**, *21*, 243–248; b) K. Yang, Q. Jing, W. Wu, L. Zhu, B. Xing, *Environ. Sci. Technol.* **2010**, *44*, 681–687.
[16] E. Müller, L. Rull, L. Vega, K. Gubbins, *J. Phys. Chem.* **1996**, *100*, 1189–1196.
[17] H. Cho, B. Smith, J. Wnuk, H. Fairbrother, W. Ball, *Environ. Sci. Technol.* **2008**, *42*, 2899–2905.
[18] B. Pan, B. Xing, *Environ. Sci. Technol.* **2008**, *42*, 9005–9013.
[19] J. Hickey, D. Passino-Reader, *Environ. Sci. Technol.* **1991**, *25*, 1753–1760.
[20] a) Y. Marcus, *J. Phys. Chem.* **1991**, *95*, 8886–8891; b) E. Vermisoglou, V. Georgakilas, E. Kouvelos, G. Pilatos, K. Viras, G. Romanos, N. Kanellopoulos, *Microporous Mesoporous Mater.* **2007**, *99*, 98–105.
[21] X. Wang, J. Lu, B. Xing, *Environ. Sci. Technol.* **2008**, *42*, 3207–3212.
[22] a) J. Liu, X. Wang, B. Fan, *Bioresour. Technol.* **2011**, *102*, 5305–5311; b) R. Walters, R. Luthy, *Environ. Sci. Technol.* **1984**, *18*, 395–403; c) S. Ahn, D. Werner, H. Karapanagioti, D. Mcglothlin, R. Zare, R. Luthy, *Environ. Sci. Technol.* **2005**, *39*, 6516–6526; d) K. Yang, X. Wang, L. Zhu, B. Xing, *Environ. Sci. Technol.* **2006**, *40*, 5804–5810; e) S. Müller, K. Totsche, I. Kogel-Knabner, *Eur. J. Soil Sci.* **2007**, *58*, 918–931.
[23] G. Cornelissen, P. Van Noort, J. Parsons, H. Govers, *Environ. Sci. Technol.* **1997**, *31*, 454–460.
[24] B. Sleep, P. McClure, *Can. Geotech. J.* **2001**, *38*, 46–52.
[25] Y. He, A. Yediler, T. Sun, A. Kettrup, *Chemosphere* **1995**, *30*, 141–150.
[26] C. N. Satterfield, *Mass Transfer in Heterogeneous Catalysis*, Krieger, Huntington, NY, **1981**, p. 18.
[27] J. W. Hamaker, J. M. Thompson in *Organic Chemicals in the Soil Environment*, *Vol. 1* (Eds.: C. A. I. Goring, J. W. Hamaker), Marcel Dekker, New York, **1972**, pp. 49–143.
[28] J. Zhang, J. Sequaris, H. Narres, H. Vereecken, E. Klumpp, *Chemosphere* **2010**, *80*, 1321–1327.
[29] M. Polanyi, *Verh. Dtsch. Phys. Ges.* **1916**, *18*, 55–80.
[30] *Monte Carlo and Molecular Dynamics Simulations in Polymer Science* (Ed.: K. Binder), OUP, Oxford, **1995**.
[31] R. Podeszwa, K. Szalewicz, *Phys. Chem. Chem. Phys.* **2008**, *10*, 2735–2746.
[32] S. D. Chakarova-Käck, A. Vojvodic, J. Kleis, P. Hyldgaard, E. Schröder, *New J. Phys.* **2010**, *12*, 013017.
[33] R. Podeszwa, *J. Chem. Phys.* **2010**, *132*, 044704.
[34] W. Hummers, R. Offeman, *J. Am. Chem. Soc.* **1958**, *80*, 1339–1339.
[35] Y. Si, E. Samulski, *Nano Lett.* **2008**, *8*, 1679–1682.
[36] G. Zhao, J. Li, X. Ren, C. Chen, X. Wang, *Environ. Sci. Technol.* **2011**, *45*, 10454–10462.
[37] Y. Sun, Q. Wang, C. Chen, X. Tan, X. Wang, *Environ. Sci. Technol.* **2012**, *46*, 6020–6027.
[38] Z. Tao, J. Zhang, J. Zhai, *Anal. Chim. Acta* **1999**, *395*, 199–203.
[39] W. Ball, P. Roberts, *Environ. Sci. Technol.* **1991**, *25*, 1223–1237.
[40] M. Dubinin, V. Astakhov, *Izv. Akad. Nauk SSSR Ser. Khim.* **1971**, *1*, 5–11.
[41] H. Sun, *J. Phys. Chem. B* **1998**, *102*, 7338–7364.

Received: April 11, 2013
Revised: May 2, 2013
Published online: August 12, 2013